Design, degradation mechanism and long-term cytotoxicity of poly(L-lactide) and poly(lactideco-ε-caprolactone) terpolymer film and air-spun nanofiber scaffold

Gad Sabbatier1,2,3, Aitor Larrañaga4, Andrée-Anne Guay-Bégin2, Jorge Fernandez4, Florence Diéval 3, Bernard Durand3, Jose-Ramon Sarasua4, and Gaétan Laroche1,2

1 Laboratoire d'Ingénierie de Surface, Centre de Recherche sur les Matériaux Avancés, Département de génie des mines, de la métallurgie et des matériaux, Université Laval, 1065, avenue de la Médecine, Québec (QC), G1V 0A6, Canada

2 Axe Médecine Régénératrice, Centre de recherche du CHU de Québec, Hôpital St François d'Assise, 10, rue de l'Espinay, Québec (QC), G1L 3L5, Canada
3 Laboratoire de Physique et Mécanique Textile, Université de Haute Alsace, École Nationale Supérieure d'Ingénieurs du Sud Alsace, 11 rue Alfred Werner 68093 Mulhouse cedex, France

4 University of the Basque Country (UPV/EHU), Department of Mining-Metallurgy Engineering and Materials Science, School of Engineering,Alameda de Urquijo s/n. 48013 Bilbao, Spain.

ABSTRACT

Degradable nanofiber scaffold is known to provide a suitable, versatile and temporary structure for tissue regeneration. However, synthetic nanofiber scaffold must be properly designed to display appropriate tissue response during the degradation process. In this context, this publication focuses on the design of a finely-tuned poly(lactide-co-e-caprolactone) terpolymer (PLCL) that may be appropriate for vascular biomaterials applications and its comparison with well-known semi-crystalline poly(L-lactide) (PLLA). The degradation mechanism of polymer film and nanofiber scaffold and endothelial cells behavior cultured with degradation products is elucidated. The results highlight benefits of using PLCL terpolymer as vascular biomaterial compared to PLLA.

KEYWORDS

Nanofibers, polylactide, poly(lactide-co-ε-caprolactone), degradation, tissue engineering, vascular biomaterials.

CITATION

Sabbatier, G., Larrañaga, A., Guay-Bégin, A. A., Fernandez, J., Diéval, F., Durand, B., ... & Laroche, G. (2015). Design, Degradation Mechanism and Long-Term Cytotoxicity of Poly (l-lactide) and Poly (Lactide-co-ε-Caprolactone) Terpolymer Film and Air-Spun Nanofiber Scaffold. Macromolecular bioscience, 15(10), 1392-1410.

This is the author's version of the original manuscript. The final publication is available at Wiley Link Online via DOI: 10.1002/mabi.201500130

1 INTRODUCTION

Vascular diseases continue to be one of the leading causes of death worldwide [1]. The autologous blood vessel remains the best option to replace coronary and peripheral arteries but is often unsuitable or simply unavailable. Accordingly, in the most serious cases of vascular diseases,

surgeons have no choice but to replace arteries with synthetic vascular prostheses. Despite the relative successfulness of woven and knitted polyethylene terephthalate (PET) and expanded polytetrafluoroethylene (ePTFE) prostheses for the replacement of larger diameter arteries (Ø > 6 mm), synthetic prostheses fail for smaller diameters (Ø < 6 mm) upon implantation in humans, because the polymeric materials exhibit a thrombogenic luminal surface leading to re-stenosis [2]. Until now, providing long-term patency small diameter vascular substitutes remains the foremost challenge in vascular surgery [3].

The current approach to improve the patency of synthetic prostheses is to regenerate a functional neo-intima on their luminal wall, therefore providing a non-thrombogenic surface between blood and prosthesis material, as observed in the native vasculature. That said, the prosthesis structure constitutes a non-suitable surface for endothelial cells (EC) monolayer proliferation due to a dimensional mismatch between the EC size and the prosthesis structure scale [4]. Consequently, covering the surface of prostheses with a nanofiber scaffold was proposed to eliminate this geometrical discordance, and allow EC proliferation as monolayer. Indeed, previous studies demonstrated that nanofiber scaffolds somewhat match the extracellular matrix fiber dimension and provide a suitable environment for cell adhesion and proliferation [5]. Nanofiber scaffold is also commonly used as the initial step for constructing a tissue-engineered blood vessel. This strategy consists of producing a spun nanofiber scaffold on a mandrel to build up a tube, which is then seeded by smooth muscle cells to regenerate the media layer, which is, in turn, cultured with endothelial cells on its internal side to reproduce the endothelium, and with fibroblasts on its external side, to get the adventitia [3]. The aforementioned approaches for generating new vascular substitutes imply the design of a spinning apparatus able to produce tubular nanofiber scaffolds as well as to coat tubular constructs with nanofiber meshes.

Most of the time, nanofiber technology is associated to the electrospinning process which has been extensively described in the tissue engineering and regenerative medicine literature in the last decades [6–9]. This common and easy route of producing nanofibers is based on the stretching of a polymer, either in solution or melted, with an electrostatic force, and enables forming uniaxially shaped objects such as ribbons [10], core-shell fibers [11], composite fibers or nanotubes [12]. These constructs can be also aligned in one or several directions as sheets or tubes according to the geometry of the collector [6,13]. In biomedical applications, nanofiber constructs find applications in bone and cartilage regeneration [14], skin regenerative medicine [15], or cardiac tissue engineering [16]. They also enable embedding bioactive molecules to mimic biological environments [17] or controlling stem cell differentiation [18,19]. Although the electrospinning process presents significant advantages, it cannot be easily used to coat small diameter vascular prostheses because of the short distance separating the needle and the surface that is intended to receive the fibers and the discontinuous textile shape of the vascular prosthesis which impedes building-up appropriate electrostatic field gradient, full jet development and solvent evaporation. To address to this issue, an alternative spinning device, called air-spinning, has been introduced by our group [5] and is continuously improved [20,21] since 2008 to coat the internal surface of vascular prostheses.

Degradable nanofiber scaffold aims to provide biomimetic morphology and a temporary support to adhesion and proliferation of cells. After the production of cell extracellular matrix and the formation of functional tissues, the scaffold is no more required and must degrade. Thus, choosing the right biomaterial with appropriate elastic properties and finely-tuned surface and degradation features is another crucial consideration for providing a biomimetic scaffold with appropriate functionalities over a predetermined period of time. In addition, the material has to be biodegradable to enable a graduate replacement by the EC extracellular matrix which is a challenge in vascular biomaterial field as well as almost every regenerative medicine strategies. Poly(α-hydroxy acid) polymers were the first biodegradable biomaterials to be implanted in humans [22]. In 1971, poly(lactide) (PLA) suture threads were approved by the Food and Drug Association (FDA). Over the years, this material was gradually replaced by poly(lactide-co-glycolide), due to its higher hydrophilic character and faster degradation rates [23]. Since then, these materials were widely

developed and used as biomedical devices because of the possibility to tune their biodegradation and mechanical properties. Indeed, these polymers are now currently used to fabricate orthopedic devices such as screws, pins, and rods, plates, and microspheres for maxillofacial surgery and drug delivery system [22]. Recently, a covalent-grafting and release model of molecules directly from PLA-based nanofiber surface was developed and demonstrated to be a promising avenue to offer suitable bioactive scaffold characteristics [24]. In vascular surgery, poly(L-lactide) (PLLA) has also been recently manufactured and marketed as bioresorbable drug-eluting stent [25]. It is possible to control the degradation rate of PLA by blending appropriate amount of this polymer stereoisomers that are poly(L-lactic acid) (PLLA), poly(D-lactic acid) (PDLA) and poly(DL-lactic acid) (PDLLA) [26]. Additionally, co-polymerization between L-lactide and ε-caprolactone units was commonly used to increase elasticity of PLA while controlling degradation rate [27]. However, the degradation of PLA blends or poly(L-lactide-co-ε-caprolactone) could evolve towards crystalline residues which are likely to remain for a long time in the body [28] and provoke immune reaction [29,30] due to an acidic degradation. A better alternative polymer was found to be a poly(lactide-co-ε-caprolactone) terpolymer (PLCL) synthesized from the copolymerization of L-lactide, DL-lactide and ε-caprolactone monomers. This novel sub-family of PLA-based materials demonstrated appropriate degradation properties for cardiovascular applications [31]. Depending on the ratio of monomers and the polymer molecular weight, the degradation rate can be modulated from some days to some months. The presence of ε-caprolactone provides the increase of the elastic properties required for cardiovascular biomaterials as compared to classical PLA blends while showing a little or even no crystalline remnants after the degradation process. Finally, this new generation of PLCL was patented in 2014 [32] and has never been spun and never studied as fibrous material.

In this context, this study aims to producing PLCL nanofiber scaffolds and studying their degradation rate and mechanisms. During all the study, PLCL was compared to semi-crystalline PLLA films and fibers in terms of degradation rate and long-term cytotoxicity. Finally, adhesion and expansion of EC were performed in contact with these materials formed as films or nanofibers and their degradation products. These experiments allowed us to ascertain the potential of PLCL to be used as vascular biomaterial and provided new information about its cytotoxicity as a function of the polymer degradation time.

2 EXPERIMENTAL SECTION

2.1 Materials synthesis

The poly(lactide-co-ε-caprolactone) terpolymer (PLCL) consisted of a statistical polymer containing 50 wt% of L-lactide, 35 wt% of D,L-lactide (>99.5%, Purac Biochem BV, Gorinchem, The Netherlands) and 15 wt% of ε-caprolactone (>98%, Merck KGaA, Damstadt, Germany) while poly(L-lactide) (PLLA) was a classical linear chain of L-lactide conformers. Both polymers were synthetized through ring-opening polymerization process, as described elsewhere [33,34]. The reaction was catalyzed by bismuth (III) subsalicylate (BiSS, 99.9 % trace metals basis, Sigma-Aldrich, 1500: 1 comonomers: catalyst molar ratio) during 24 h at 130 °C.

2.2 Films and nanofibers

PLCL and PLLA films were processed by compression molding in a Collin´s P200E hydraulic press (at 210 ºC and 24 MPa for PLLA films and at 180 ºC and 24 MPa for PLCL films) to obtain squared films (11 cm x 12 cm). Films were then quenched in water in order to promote the formation of an amorphous state. Finally, PLLA films were crystallized during 100 min at 120 °C in an oven to reach a crystallinity degree equivalent to the PLLA polymer before film processing. Each film was washed two times in water in ultrasonic bath for 10 min each.

Polytetrafluroethylene (PTFE) films were obtained from Goodfellow (Coraopolis, PA, USA) and used as negative control in cells culture assays. PTFE films were punched with an 8 mm-diameter pastry cutter and sequentially washed for 10 min in acetone, water and ethanol in an ultrasonic bath to remove impurities and stored in vacuum at least 72 hours.

PLCL and PLLA were also totally dissolved in chloroform (99.8%, Laboratoire Mat, Québec, QC, Canada) at room temperature and spun with an air-spinning device previously described elsewhere [20]. An optimal polymer concentration of 14wt% was calculated from the viscosity of the polymer solution for both PLCL and PLLA and, accordingly, the needle diameter (0.41 mm), syringe pump flow rate (10 mL/h), air pressure (7.5 MPa) and needle-collector distance (250 mm) were set. Nanofibers were then stored under vacuum at least 72 h to remove all trace of solvent.

2.3 Polymer degradation procedures

For the in vitro degradation study, PLCL and PLLA square samples (1 cm x 1 cm) taken from films and air-spun nanofibers (groups 1 to 8 in Table 1, n = 3) were weighted (W0) and totally immersed in Falcon tubes containing a phosphate buffered saline (PBS) (pH = 7.4, Sigma Aldrich, St. Louis, MO, USA) solution. The volume was adjusted to get a mass to volume ratio of 1 g/L. Each sample was placed in an oven at 37°C for 70 days.

Table 1. List of sample groups

Sample groups	Material	Shape	Degradation temperature (°C)
1	PLCL	film	No degradation
2	PLCL	Fibers	No degradation
3	PLLA	film	No degradation
4	PLLA	Fibers	No degradation
5	PLCL	film	37
6	PLCL	Fibers	37
7	PLLA	film	37, 50
8	PLLA	Fibers	37, 50
9*	PLCL	Film degradation product 1 g/L	37
10*	PLCL	Fiber degradation product 1 g/L	37
11*	PLCL	Fiber degradation product 5 g/L	37
12*	PLLA	Film degradation product 1 g/L	37, 50
13*	PLLA	Fiber degradation product 1 g/L	37, 50
14*	PLLA	Fiber degradation product 5 g/L	37, 50

Accelerated degradation studies were also performed on PLLA film and fiber samples (groups 7 and 8 in Table 1, n = 3) in order to obtain the same degradation rate between PLCL at 37°C and 70 days of degradation and PLLA to provide a better comparison between the two materials. Conditions of accelerated degradation applied to PLLA were determined from models described by Weir et al. [35]. Accordingly, PLLA fiber and film samples were kept in PBS at 50°C during 120 days with mass to volume ratio of 1 g/L.

For studying EC behavior while seeded on materials submitted to the aforementioned degradation procedures, degradation process was performed in autoclaved distilled water with the same groups of samples (groups 1 to 8 in Table 1, 37 and 50°C, n = 3). Water was used as degradation medium instead of PBS to preserve an appropriate osmolarity for cell culture medium. Film samples were punched (8 mm-diameter) with a pastry cutter before degradation to match the well dimension of 48-well plates. The sample weight to liquid volume ratio was adjusted at 1 g/L and

at 5 g/L to assess the effect of degradation product concentration on cell survival (groups 9 to 14 in Table 1, n = 3).

2.4 Molecular characterization of synthesized PLCL

The characterization of PLCL after synthesis is described in supporting information and was detailed in a previous publication [36]. Briefly, the molecular structure of PLCL was determined from proton nuclear magnetic resonance (1H-NMR) spectra recorded with a Bruker Avance DPX 300 (Billerica, MA, USA) at 300 MHz using 5 mm diameter sample tubes. Peaks at 5.15 ppm and 4.1 ppm, assigned to methine of lactide and methylene of ε-caprolactone, respectively, allowed the statistical calculation of ratios related to different polymer conformation (Figure S1). Lactide and ε-caprolactone relative molar contents were determined from the ratio of the aforementioned integrated intensities. From these values, the number-average sequence lengths of lactide (l_{LA}), L-lactide (lL LA), D-lactide(lD-LA), and ε-caprolactone (l_{CL}) units and the randomness character (R) were calculated according to and previously published procedure [33] detailed in supporting information.

2.5 Characterization of polymer films before degradation

Tensile testing was performed on PLCL and PLLA films after processing. Tensile mechanical properties were determined with an Instron 5565 dynamometer (Instron, Nordwood, MA, USA) at a crosshead speed of 10 mm/min. These experiments were performed according to the ISO 527-3/1995 standard procedure at both room temperature (21 ± 2°C) and 37 °C. For the experiments made on PLCL films at 37 °C, the elastic modulus was calculated from the strain at 10 % using a secant at 2 % strain since no yield point was observed in the stress-strain plot. In addition, the tensile strength was measured after 300 % of strain, which corresponds to the maximum distance physically achievable between the clamps at 37 °C. For all other samples, the elastic modulus was considered as a Young's modulus (PLLA) or a secant modulus at 2 % (PLCL), while the tensile strength was determined after sample failure.

The thickness of PLCL and PLLA films was determined before degradation using a profilometer (DektakXT Advanced system, Bruker) equipped with a 12.5 µm tip. A force of 3 mN was applied from the tip to the surface. The acquisition lasted 60 s on a distance of 500 µm.

Contact angle measurements were performed on film samples using a VCA 2500 XE system (AST, Billerica, MA, USA). Three 3 µL drops of distilled water were set down on film surfaces and the contact angle was calculated with VCA Optima software.

2.6 Physical and chemical characterization during degradation

At different periods of time, samples (n = 3) of each in vitro degradation group of samples were removed from the PBS and weighed wet (W_w) after wiping the surface with a filter paper to adsorb the excess of water. These samples were air-dried overnight and then vacuum-dried for 24 h. They were weighed again to obtain the dry weight (W_d). Water absorption (%WA) and remaining weight (%RW) were calculated according to Equation (1) and (2).

$$\%WA = \frac{W_w - W_d}{W_d} \times 100 \quad (1)$$

$$\%RW = \frac{W_d}{W_0} \times 100 \quad (2)$$

The molecular weight evolution of the samples during hydrolytic degradation was determined by GPC using a Waters 1515 GPC apparatus (Milford, MA, USA) equipped with two Styragel columns with pore size ranging from 10^2 and 10^4 Å. Chloroform was used as an eluent at a flow rate of 1 mL

min^{-1} while polystyrene standards (Shodex Standards, SM-105) were used to obtain a calibration curve (Figure S2).

The thermal properties were determined on a DSC 2920 (TA Instruments, New Castle, DE, USA). Samples of 5-10 mg were heated at 20 ºC.min^{-1} from -20 ºC to 210 ºC for PLLA samples and from -85 ºC to 185 ºC for PLCL samples. This first scan was used to determine the melting temperature (T_m), the heat of relaxation (ΔH_r), the heat of crystallization (ΔH_c) and the heat of fusion (ΔH_m) of the samples. After this first scan, the samples were quenched in the DSC at the input beginning temperature and a second scan was performed using the same heating conditions. The data from this second scan were used to measure the glass transition temperatures (T_g), which was determined from the inflection point of the heat flow curve. Then, the crystallinity degree (χ) of semi-crystalline samples was calculated according to Equation (3):

$$\chi = \frac{\Delta H_m - \Delta H_c}{\Delta H_m^0} \times 100 \quad (3)$$

Where $\Delta H_m^0 = 106\, J/g$ [37] is the melting enthalpy for a 100% crystalline PLLA sample.

The samples were then gold-coated and observed under a scanning electron microscope (EVO® 50, Carl Zeiss, Göttingen, Germany) (SEM) equipped with an Everhart-Thornley secondary electron detector at a 10 kV accelerating voltage. Images were analyzed with image treatment software (Image J, National Institutes of Health, Bethesda, MD, USA). Fiber diameter of PLLA and PLCL fibrous samples were measured on images with a magnitude of 10000 or 15000. A total of approximately 120 fiber diameter measurements were randomly made for PLCL fibrous sample before and after 3 days of degradation and 150 fiber diameter measurements for PLLA nanofibers before and after 35, 70 and, and 120 days of degradation, either at 37°C and 50°C. Fiber diameter distribution was normalized and fitted with three parameter lognormal function (Equation (4)) using Sigma Plot software (Sigma Plot 11.0, Systat Software Inc., San Jose, CA, USA).

$$y = \frac{k}{x - x_0} e^{-\left(\frac{\ln(x - x_0) - \ln(\mu)}{2\ln(\sigma)}\right)^2} \quad (4)$$

In this equation, k is the proportionality constant, x_0 is the shift parameter, μ is the geometrical mean of the fiber diameter, and σ is the geometrical standard deviation, called shape parameter. The progression of the mode, which is the fiber diameter value corresponding to the maximum of the lognormal curve, provided dimensional information about the degradation mechanisms. For instance, a decrease of the mode of the lognormal curve means that fiber diameter decreases upon degradation while an increase of this parameter rather signifies that fiber diameter gets higher under the influence of degradation mechanisms such as scaffold shrinkage or fiber diameter inflation. The shape parameter, which describes the curve asymmetry, highlights which of the low or high diameter fibers are more affected by the degradation process. A shape parameter value close to 1 is characteristic of a Gaussian curve, meaning that the fiber diameter population is equally distributed around the mode (which is also the mean in the case of a symmetric distribution).

2.7 HSVEC isolation and culture

HSVECs were isolated from healthy human saphenous vein segments removed during varicose vein stripping surgeries as previously described [38]. All procedures were approved by the CHU de Québec ethics committee and with the informed consent of donors at the Saint-François d'Assise Hospital in Québec city. After isolation, cells were frozen in 90 % fetal bovine serum (FBS) and 10 % dimethyl sulfoxide (DMSO). For all experiments, HSVECs were thawed after passage 2 and maintained in tissue culture treated t-flasks (Corning, NY, USA) in complete culture medium. The

complete culture medium consisted of M199 medium (M199 powder, Life technologies, Burlington, ON, Canada) supplemented with 20 % of FBS (Thermo Fisher Scientific, Waltham, MA), 50 units/mL heparin, 10 ng/mL basic fibroblast growth factor (bFGF, amino acids 10-155), 100 units/mL penicillin and 100 µg/mL streptomycin (all from Life Technologies).

2.8 Preparation of samples for HSVEC seeding, validation of sanitization procedures and pH measurements

Samples from group 1 to 4 (Table 1) and PTFE films were positioned in wells of standard tissue culture 48-well plates (Corning) with 0.4 cm² homemade sterile glass culture cylinders and immersed in sterile distilled water containing 500 units/mL of penicillin and 500 µg/mL of streptomycin for 24h to prevent bacterial formation. Finally, samples were washed 2 times with sterile distilled water and dried under sterile conditions overnight at room temperature.

Procedures to avoid bacterial formation were validated with bacterial and fungus culture experiments. Each group of samples were sanitized using the aforementioned method and immersed in complete culture medium for 2 days. A blank well was used as control. Then, 10 µL of the medium was taken from each sample and spread on a Petri dish covered with agarose. Finally, Petri dishes were incubated for 8 days and observed after experiments (Figure S3).

Water containing degradation residues (group 9 to 14 in Table 1) were stored at 4 °C and sterilized by autoclaving at 121 °C during 45 min. The pH of these samples was then measured with a pH meter (Accumet™ 25, Fisher Scientific, Canada) at room temperature. Also, the measurement was repeated after mixing the liquid samples with two-time concentrated M199 solution at a 1:1 ratio. Sterile water and one-time concentrated M199 were used as control.

2.9 HSVECs adhesion and proliferation experiments in function of degradation

For adhesion and expansion experiments before degradation, control samples consisted of a blank polypropylene (PP) wells treated for cell culture (positive) and PTFE films (negative), which is anti-adhesive due to its hydrophobicity. Moreover, a well was treated with gelatine during 20 min to be used as second positive control sample in adhesion assays. Samples were seeded with 75 000 cells/cm² (adhesion tests) or 20 000 cells/cm² (proliferation tests) HSVECs in complete medium and were incubated at 37 °C with 5 % of carbon dioxide (CO_2) for 1 hour and a half or for 48 h and 96 h, respectively. For sample groups from 9 to 14, complete medium with two-time concentrated M199 was prepared and mixed with an appropriate volume of water-containing degradation products. In this case, another negative control (cytotoxic medium) consisted of mixing two-time concentrated M199 with DMSO instead of water was prepared. After the incubation, medium was pumped, and samples were rinsed 2 times with PBS. Then, 500 µL of 90% M199 medium and 10% resazurin (Life Ttechnologies) solution at 250 ug/mL was poured on the samples. After 3h of incubation, 300 µL of the culture media was taken from each well and transferred in another well plate for further fluorescence measurements. A spectrofluometer (FL600 fluorescent microplate reader, Bio Tek, Winooski, VT, USA), equipped with 530 nm excitation source and a 590 nm emission output filter was used to record the fluorescence emission intensity of resorufin resulting from the metabolization of resazurin by cells. The fluorescence level was then compared with a calibration curve in the same well plate. This calibration curve was performed by measuring the emission level of resorufin with different level of dilution. Moreover, the noise of measurement was subtracted from the fluorescence signal by quantifying the emission level of a blank well containing a rezasurin solution (90 % M199 medium and 10 % resazurin solution at 250 ug/mL). The data consisted of the mean of 9 measurements recorded at different locations in the well. The adhesion results were normalized to the blank-well positive control and the expansion results to initial number of adhered cells in a blank PS well at 20 000 cells/cm². Each experiment was made triplicate.

3 RESULTS

3.1 Initial characterization of PLCL and PLLA

The global and micro structure of the synthesized polymers (PLLA and PLCL) [33] as well as their general mechanical and thermal properties were characterized and are presented in Table 2.

Table 2. Characteristics of PLLA and PLCL films

	Features		PLCL	PLLA	Technique
Structural properties	M_w (x10^3)		101.6 g.mol^{-1}	102.4 g.mol^{-1}	GPC
	dispersity index (*D*)		1.7	1.5	
	Composition	%L-lactide	66.9 %	100 %	^{1}H-NMR (Equation (S1), (S2) and (S3))
		%D-lactide	17.4 %	-	
		%ε-caprolactone	15.7 %	-	
Microstructural magnitudes*	I_{LA}		6.68	-	
	$I_{L\text{-}LA}$		3.18	-	
	$I_{D\text{-}LA}$		1.27	-	
	I_{CL}		1.25	-	
	R		0.95	-	
Physical properties	T_g		34 ºC	57 ºC	DSC
	T_m		-	181 ºC	
	X_c		-	42%	DSC (Equation (3))
	Thickness of film (μm)		(16 ± 2) × 10^1	(18 ± 2) × 10^1	Profilometer
Mechanical properties	Elastic modulus (MPa)	21 ºC	(76 ± 7) × 10^1	(181 ± 2) × 10^1	Dynamometry
		37 ºC	11 ± 1	(142 ± 7) × 10^1	
	Yield strength (MPa)	21 ºC	21 ± 2	-	
		37 ºC	0.7 ± 0.1	38 ± 2	
	Tensile strength (MPa)	21 ºC	17 ± 1	56 ± 2	
		37 ºC	1.6 ± 0.1	20 ± 1	
	Elongation at break	21 ºC	(35 ± 4) × 10^1 %	4.0 ± 0.3 %	
		37 ºC	>300 %	37 ± 2 %	
Surface properties	Contact angle		74 ± 3 °	84 ± 6 °	Contact angle measurement device

As expected, PLLA and PLCL films have very similar molecular weight and dispersity indexes that are confirmed by GPC measurements (table 2). The synthesized PLLA is semi-crystalline and shows a brittle behavior at 21 °C that becomes more ductile at 37 °C. However, PLCL is completely amorphous. The high randomness of conformational arrangements, characterized by the randomness character value (R) close to 1, along with the incorporation of D-lactide, which disorders the microstructural arrangements of crystallizable L-lactide, lead to the shortening of its average

sequence length ($l_{L\text{-}LA}$ = 3.18). The presence of ε-caprolactone improves the viscoelastic properties of the synthesized material, avoiding the brittleness related problems as compared to PLLA. In this sense, the synthesized terpolymer exhibits a glassy thermoplastic behavior at room temperature. On the contrary, at body temperature, (37 °C) the material behaves as a thermoplastic elastomer (TPE) with a low secant modulus. The working temperature (37 °C) being above the T_g (34 °C), it leads to a higher mobility of polymer chains and explains these remarkable elastic and viscoelastic property improvements in contrast with results from mechanical experiment performed at 21°C. Finally, the surfaces of both PLCL and PLLA films exhibit very similar contact angle values, therefore putting in evidence almost identical hydrophilicity character.

3.2 GPC and mass measurement results versus degradation time

Figure 1 shows molecular weight (M_w) data measured using GPC (Figure 1a), kinetic constants and half-life times calculated using a first-order reaction model (Equation (5) and Equation (6); Figure 1b).

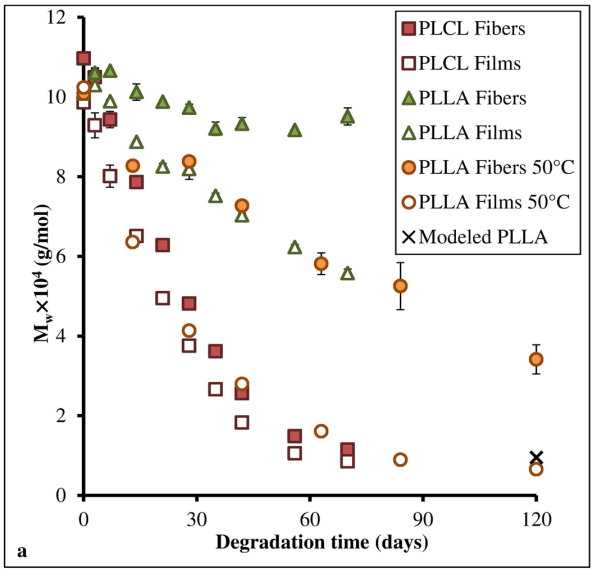

Materials	Temperature (°C)	|k| values (d^{-1})	$t_{1/2}$ (d)
PLCL Fibers	37	3.5×10^{-2}	20.0 ± 0.2
PLCL Films	37	3.8×10^{-2}	18.2 ± 0.1
PLLA Fibers	37	1.9×10^{-3}	(36 ± 6) x 10^1
PLLA Films	37	8.9×10^{-3}	77.9 ± 0.8
PLLA Fibers	50	8.6×10^{-3}	81 ± 2
b PLLA Films	50	2.9×10^{-2}	23.9 ± 0.2

Figure 1. GPC measurement results, (a) Molecular weight as a function of the degradation time and (b) Half-life degradation times.

As expected, PLLA samples degrade slower at 37 °C than PLCL samples. PLLA films and fibers exhibit a loss of 45 % and 3 % of their Mw after 70 days of degradation, respectively, whereas PLCL samples show a decrease of around 90 % for both films and fibers (Figure 1a). Additionally, these molecular weight measurements indicate that films degrade faster than fibers for all investigated samples.

A first order degradation kinetics, known to appropriately describe bulk hydrolysis reaction of degradable polyesters [39], is used to determine the relationship between polymer molecular weights and degradation time. Accordingly, equations (5) and (6) are used in order to compare and quantify degradation rates.

$$-\frac{d(M_w)}{dt} = k(M_w) \Rightarrow ln(M_w) = -kt + ln(M_{w0}) \quad (5)$$

$$t_{1/2} = \frac{ln2}{|k|} \quad (6)$$

Where M_w is the weight-averaged molecular weight, M_{w0} is the initial weight-averaged molecular weight, k is the apparent degradation rate and $t_{1/2}$ is the half-life time of degradation. The calculation of k-values was performed by the fitting $ln(M_w)$ in function of time curve with a linear regression using an exponential relationship.

Figure 1b reports the results of these regressions, which quantify the polymer degradation rate. Half-life times calculated from the kinetics curve ($t_{1/2}$) of the degradation reaction of PLLA degraded at 50 °C are 3.3 to 4.5 times lower than those measured at 37 °C. Moreover, modeling of the polymer degradation rate, calculated using the model developed by Weir et al [35], is in agreement with our experimental degradation data measured on films. PLCL films degraded at 37 °C for 70 days and PLLA films degraded at 50 °C for 120 days show slightly different molecular weights, respectively (85 ± 2) x 10^2 g/mol and (66 ± 5) x 10^2 g/mol, and half-life time degradation respectively 18.2 ± 0.1 days and 23.9 ± 0.2 days.

Finally, M_w measured at the end of degradation, as well as $t_{1/2}$ values are similar for both PLCL films and fibers degraded either at 37 °C. On the opposite, the PLLA degradation rate profile strongly depends on the shape of the polymer samples as both films and fibers exhibit a completely different behavior, either at 37 °C or 50 °C.

As observed in Figure 2a, PLLA films and nanofibers do not experience significant weight loss during the course of the study. However, PLCL samples maintain their initial mass until 56 days of degradation, followed by a sharp mass decrease of about 30 % after 70 days. This mass loss in PLCL samples is accompanied by a significant increase of water absorption (Figure 2b).

As seen in Figure 2b, the water absorption of nanofibers is initially higher than the water absorption in films because of their higher surface to volume ratio. For example, the water absorption for PLCL films at day 3 was 5 ± 1 % whereas it is of 34 ± 4 % for PLCL nanofibers. However, after 56 days of immersion in PBS, the water absorption of PLCL films is clearly higher than that of PLCL nanofibers due to their more advanced degradation state. In addition, it has to be pointed out that water absorption of PLLA nanofibers is clearly higher than PLCL nanofibers.

In summary, Figures 1 and 2 put in evidence a polymer Mw decrease concomitant with a constant overall weight for PLLA samples and a sharp decrease for PLCL samples after 56 days of degradation at 37°C, therefore pointing to a bulk degradation mechanism. In addition, these data also demonstrate that PLCL degraded faster than PLLA and that fibers degraded slower than films.

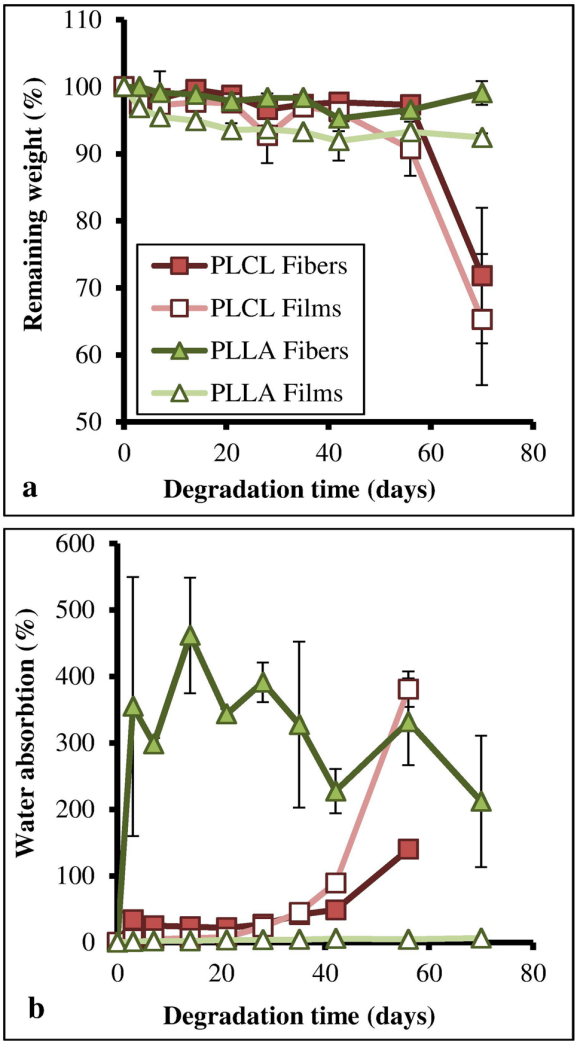

Figure 2. Mass measurements results, (a) Remaining weight and (b) Water absorption as a function of the degradation time at 37°C in PBS.

3.3 Thermal analysis versus degradation time

Figure 3 presents the first DSC runs for PLLA films and fibers degraded at 37 °C (Figure 3a and Figure 3b) and at 50 °C (Figure 3c and Figure 3d) and T_g calculated from the second DSC runs and X_c values for PLLA samples (Figure 3e).

PLLA films degraded at 37 °C (Figure 3a) display a melting peak at 186 °C before degradation, with a progressive shift towards 176 °C upon degradation and a gradual increase of their crystallinity index (X_c) from 47 % to 61 % (Figure 3e). In addition, the T_g measured on the 2nd run of DSC (Figure 3e) exhibits a decrease from 56.7 °C to 47.6 °C during the degradation. These changes in PLLA are related to the reduction in molecular weight that leads to a decrease in molecular entanglement and an increase in chain mobility. Due to this higher mobility, the chains could reorganize themselves into a more ordered macromolecular arrangement and, accordingly, the crystallinity of PLLA increased. Moreover, since the hydrolysis occurs preferentially in amorphous regions, an increase of crystallinity of PLLA samples with degradation time is expected. These degradation behaviors are further catalyzed at higher temperatures (Figure 3c). For example, upon degradation at 50 °C, the crystallinity index can reach values as high as 83 % at day 63 and 90 % after 120 days of degradation (Figure 3e).

PLLA nanofibers show completely different DSC thermograms. As can be seen in Figure 3b, an endothermic peak is observed for PLLA samples degraded at 37 °C, overlapping with the glass transition, which can be associated to an enthalpic relaxation peak. Moreover, an exothermic peak appears between 80 °C and 100 °C indicating a cold crystallization and a reorganization of the PLLA nanofibers structure during the heating process. Finally, little changes are observed in these thermograms as a function of degradation time. Indeed, both T_m and X_c remain almost constant at around 180 °C and 30 %, respectively.

As opposed to the experiments performed at 37 °C, degradation of PLLA nanofibers at 50 °C lead to major changes in these samples DSC thermograms (Figure 3d). Indeed, the enthalpic relaxation as well as cold crystallization peaks disappears as a result of immerging the PLLA samples in an aqueous environment at a temperature close to their glass transition temperature. So, it is likely that chain scissions during degradation lead to a progressive decrease of T_g. Above this transition temperature, polymer chains are mobile and able to form crystalline phases, through a mechanism similar to the cold crystallization process, previously described. Relaxation and cold crystallization processes are non-reversible transitions, therefore explaining their absence in the DSC thermograms after 28 days of degradation (Figure 3d). Accordingly, cold crystallization vanishing during degradation leads to a drastic rise of the polymer crystallinity index, increasing from 27 % for PLLA fibers before the degradation to 53 % after day 28. Finally, the increase of the index of crystallinity from 28 days to 120 days arises due to the degradation of the amorphous phases.

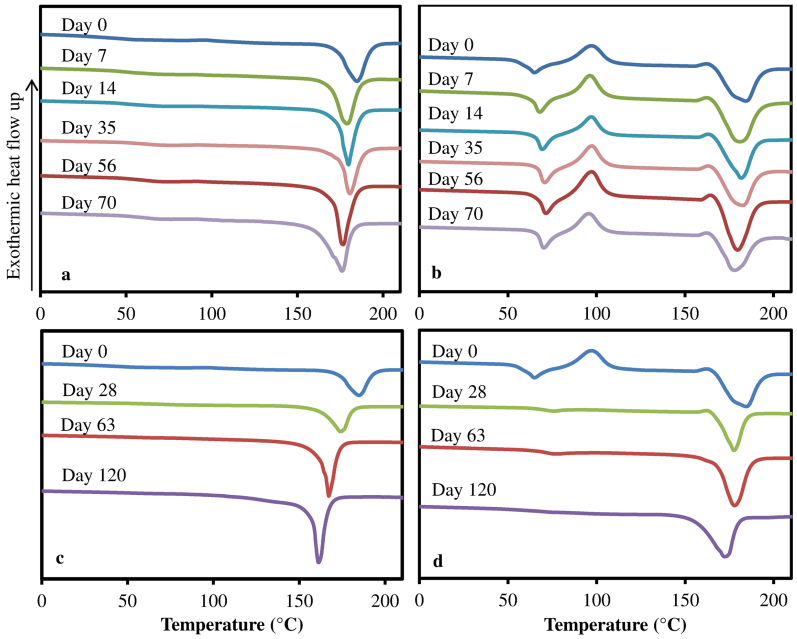

e **Features of PLLA samples**

Degradation Temperature	Degradation Time (d)	Fibers		Films	
		Tg (°C)	Xc (%)	Tg (°C)	Xc (%)
37°C	0	57.2	27	56.7	47
	7	55.0	27	51.5	51
	14	57.0	29	49.8	59
	35	56.9	26	54.4	55
	56	58.6	30	51.2	59
	70	51.8	26	47.6	61
50°C	28	51.0	53	54.2	64
	63	54.9	58	44.3	83
	120	49.7	61	49.7	90

Figure 3. DSC thermograms of PLLA film samples degraded at 37°C (a), PLLA fiber samples degraded at 37°C (b), PLLA film samples degraded at 50°C (c), PLLA fiber samples degraded at 50°C (d) and T_g and X_c of PLLA samples (e).

Figure 4 exhibits DSC thermograms of PLCL nanofibers as a function of degradation time. The absence of melting peaks highlights the fact that PLCL fibers are amorphous before the hydrolysis process and remain amorphous up to the end of degradation. Moreover, no enthalpic relaxation peak is observed since the temperature of degradation was above the T_g. In addition, the decrease of T_g values from 35.0 °C at day 0 to 27.8 °C after day 70 could also be associated to the presence of shorter chains with higher mobility. It should also be pointed out that the PLCL nanofiber thermograms presented therein are similar to those of PLCL film previously published [33].

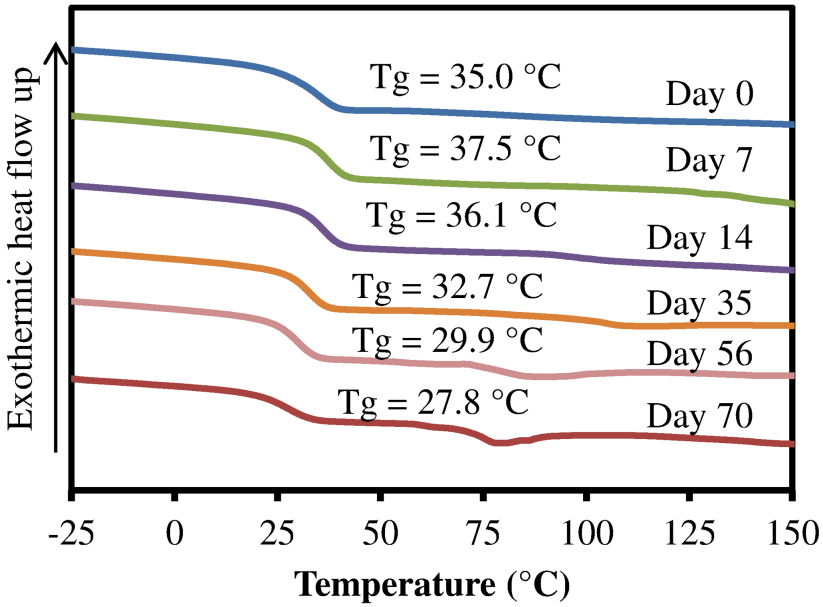

Figure 4. DSC thermograms of PLCL fiber samples degraded at 37°C

3.4 Morphology of samples as a function of degradation time

Figure 5 shows PLLA nanofibers morphologies before and after 35, 70 and 120 days of degradation at 50 °C, as visualized by SEM, along with the log-normal fitting of fiber diameter distribution. The R^2 value indicates the correlation between the experimental and the predicted values (Figure 5g).

At day 0, nanofiber scaffolds display typical fibrous morphology that is produced by the air-spinning device (Figure 5a). The surface proportion covered by the fibers is largely over 90 % which confirms the choice of the setting parameters previously identified in a former article [20]. In addition, the distribution of fiber diameters can be correlated with a lognormal curve (R^2 = 0.90) displaying a maximum peak at 290 nm.

On the contrary, PLLA nanofibers degraded at 50 °C undergo important modification. First of all, the macroscopic visualization of fibers demonstrates a fibrous state at day 35 (Figure 5b). However, the fibers crumble at day 70 showing a powder-like morphology (results not shown) that is further confirmed by SEM observation (Figures 5c). Then, Figure 5e indicate that the size of these remnants become smaller after 120 days. In addition, enlarged views (Figure 5d and Figure 5f) evidence these samples, consisting of fiber fragments, were split during the degradation. Then, the mode of fiber diameters (Figure 5g) decreases from 290 nm before the degradation to 229 nm at day 35, 176 nm at day 70, and 191 nm at day 120. Finally, the shape parameter decreases with the degradation time, displaying values of 1.55 before the degradation and 1.35 at day 35, 1.32 at day 70, and 1.28 at day 120. Besides to indicate a smaller diameter of fibers, the evolution of these parameters allows

measuring a sharper distribution of fiber diameter with modes moving towards lower values with the degradation time.

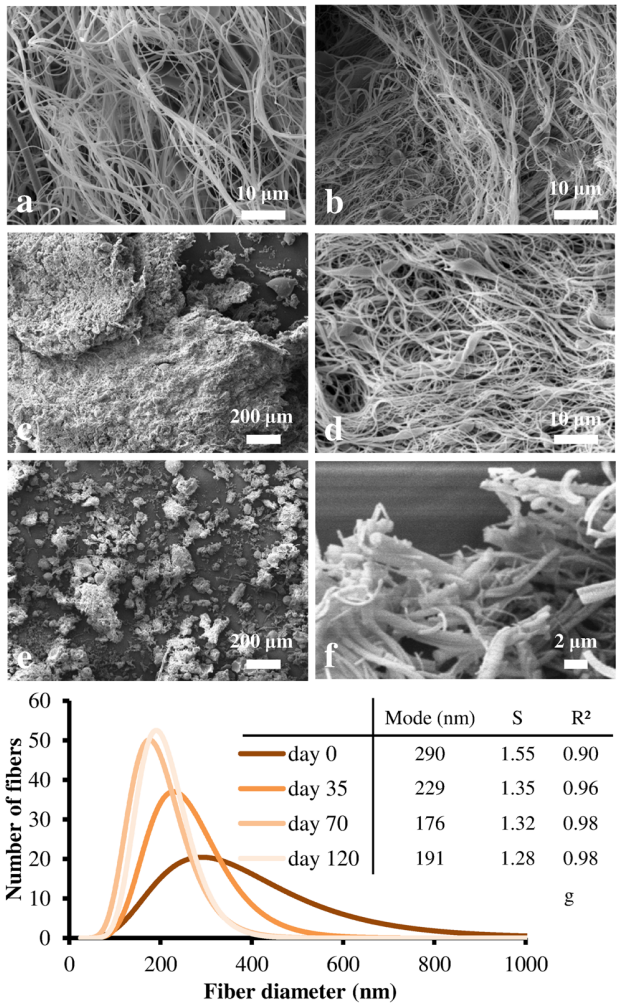

Figure 5. SEM images showing the evolution of PLLA nanofibers structure with accelerated degradation at 50°C, PLLA nanofiber scaffold before degradation (5000x) (a), PLLA nanofiber scaffold at day 35 (5000x) (b), PLLA nanofiber scaffold at day 70 (200x) (c), PLLA nanofiber scaffold at day 70 (5000x) (d), PLLA nanofiber scaffold at day 120 (200x) (e), PLLA nanofiber scaffold at day 120 (15000x) (f), Lognormal fitting of fiber diameter distribution (g). R^2 is the correlation factor between the fiber diameter distribution and the log-normal function and S is the shape parameter.

After 120 days of degradation at 37 °C, the mode of the distribution curve measured from the PLLA nanofiber diameters do not change significantly. Also, the morphology of fibers is not modified, as measured either by optical microscopy or SEM images (not shown). However, the shape parameter of the lognormal curve decreases with the degradation time.

Figure 6 illustrates the evolution of PLCL nanofibers morphology before and after 3, 35, and 70 days of degradation at 37 °C, as visualized by SEM. Additionally, the log-normal curve fitting of fiber diameter distribution is shown in Figure 6g.

Before degradation, PLCL nanofiber scaffold presents the same non-woven fibrous morphology (Figure 6a) than PLLA nanofiber scaffold with a higher mode (553 nm vs 290 nm, respectively). Besides, the shape parameter, which is close to 1 (1.39), is indicative of a more symmetric fiber diameter distribution as compared to that of the PLLA scaffold (1.55; Figure 5g).

After 3 days of degradation, fibers swell and some parts of the sample show that nanofibers have merged (Figure 6b) leading to a global shrinkage of the scaffold. As a result, the mode of fiber diameter increases until 854 nm, with a wider distribution. Accordingly, the swelling of each fiber size population is characterized by a lower shape parameter (1.33).

At day 35, sample has totally shrunk (Figure 6c); fibers merge to produce a smooth surface and a porous core (Figure 6d). At day 70, the sample is glassy (Figure 6e and Figure 6f) and have the same morphology than a PLCL film (results not shown).

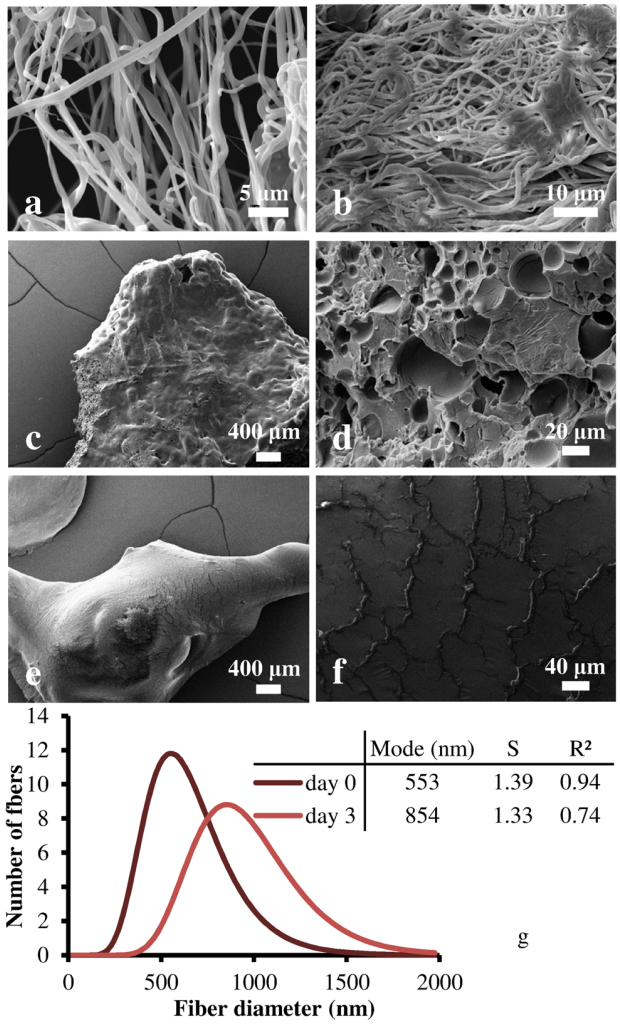

Figure 6. SEM images showing the evolution of PLCL nanofibers structure with degradation at 37°C, PLCL nanofiber scaffold before degradation (10000x) (a), PLCL nanofiber scaffold at day 3 (5000x) (b), PLCL nanofiber scaffold at day 35 (200x) (c), PLCL nanofiber scaffold at day 35 (5000x) (d), PLCL nanofiber scaffold at day 70 (200x) (e), PLCL nanofiber scaffold at day 70 (5000x) (f), Log-normal fitting of fiber diameter distribution (g). R^2 is the correlation factor between the fiber diameter distribution and the log-normal function and S is the shape parameter.

3.5 pH measurements

Table 3 presents pH measurement results of group 9, 10 and, 11 samples at 37 °C and group 12, 13 and, 14 samples at 37 °C and 50 °C (see Table 1 for sample description). The pH was

measured in sterile distilled water in which the samples are degraded and consequently, the solutions in which the measurements were performed consisted of water and the degradation products.

First of all, the medium containing degradation products become acidic for every sample during degradation, which could potentially lead to an autocatalysis of the degradation. This is because the hydrolysis of PLA based polymer ester bonds leads to the formation of acidic by-products and consequently, to a pH decrease.

At day 35, the pH of the aqueous solution containing the PLLA film at 37 °C is higher than pH of PLLA fibers in the same conditions. However, in the case of solutions containing PLCL at 1 g/L, the pH variation upon degradation is almost similar for films and fibers. At 50 °C, the pH of the aqueous solution containing the PLLA film is significantly lower than that of the solution containing PLLA fibers. Moreover, samples degraded with a mass to volume ratio of 5 g/L have, of course, a lower pH than samples with a ratio of 1 g/L, highlighting a higher concentration of acidic by-products. Mixed at a 1:1 ratio with the M199 buffered culture medium, these aqueous solutions lead to pH ranging between 7.1 and 7.6, suitable for endothelial cell culture.

At day 70, a slight but significant drop of pH values is observed for all samples as compared to their counterpart at day 35, indicating that more degradation occurs. Solutions mixed with M199 and containing PLLA film at 50 °C and 1 g/L or PLLA fibers at 50 °C and 5 g/L lead to pH values of 6.84 and 6.49, respectively.

Table 3 showed that no major changes in pH occurs after 120 days of degradation in water as compared with measurements made at day 70, except for PLLA films at 37 °C and 1 g/L and PLLA fibers at 50 °C and 5 g/L that demonstrates a significant decrease.

Finally, the comparison between PLLA at 50 °C and PLCL at 37 °C highlights that acidic by-products released from degradation of caprolactone units are less acidic than those released from degradation of lactide units for the same degradation rate.

Table 3. pH measurements in water and in M199 medium

Samples	pH of the degradation medium (in water)			pH of the degradation solution and M199 medium (ratio 1:1)		
	Day 35	Day 70	Day 120	Day 35	Day 70	Day 120
Water	6.0 ± 0.2			-		
M199	-			7.42 ± 0.01	7.36 ± 0.01	7.46 ± 0.01
PLLA film 37°C 1g/L	4.6 ± 0.2	4.3 ± 0.2	3.7 ± 0.1	7.52 ± 0.01	7.49 ± 0.04	7.61 ± 0.05
PLLA fibers 37°C 1g/L	4.13 ± 0.04	4.05 ± 0.03	4.06 ± 0.04	7.52 ± 0.04	7.47 ± 0.02	7.65 ± 0.01
PLLA fibers 37°C 5g/L	3.81 ± 0.01	3.61 ± 0.01	3.61 ± 0.06	7.46 ± 0.00	7.51 ± 0.06	7.66 ± 0.02
PLLA film 50°C 1g/L	3.26 ± 0.08	3.11 ± 0.09	3.1 ± 0.1	7.1 ± 0.1	6.84 ± 0.05	6.88 ± 0.05
PLLA fibers 50°C 1g/L	3.7 ± 0.2	3.5 ± 0.2	3.1 ± 0.1	7.43 ± 0.07	7.30 ± 0.02	7.1 ± 0.1
PLLA fibers 50°C 5g/L	3.21 ± 0.02	2.93 ± 0.01	2.86 ± 0.01	7.10 ± 0.02	6.49 ± 0.05	6.85 ± 0.03
PLCL film 37°C 1g/L	4.15 ± 0.05	3.8 ± 0.2	-	7.57 ± 0.03	7.46 ± 0.03	-
PLCL fibers 37°C 1g/L	4.10 ± 0.01	4.0 ± 0.1	-	7.51 ± 0.04	7.48 ± 0.03	-
PLCL fibers 37°C 5g/L	3.73 ± 0.01	3.63 ± 0.04	-	7.44 ± 0.01	7.43 ± 0.04	-

3.6 HSVEC adhesion and expansion before degradation

HSVEC adhesion (1h 30; Figure 7a) and proliferation (2 and 4 days; Figure 7b) results are obtained from the fluorescence measurement of resorufin, which is the cell metabolization product of rezasurin.

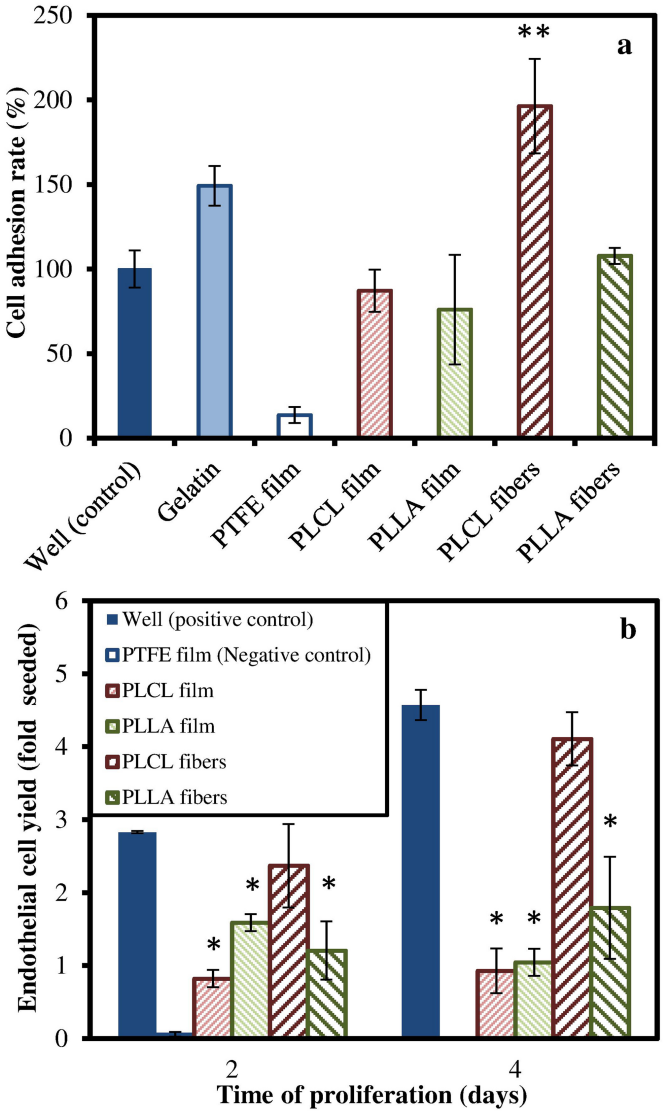

Figure 7. Adhesion (a) and expansion (b) of HSVEC before the degradation process (day 0). * = significant difference ($p < 0.05$) as compared to the PP treated well according to Krurskal-Wallis ANOVA test. ** = significant difference ($p < 0.05$) as compared to a gelatinized well.

Figure 7a demonstrates that the adhesion of HSVEC to PLLA and PLCL films is not statistically different from that observes in the PP treated well. However, PLCL fibers reveal to be very adherent surfaces, even resulting in a better outcome than gelatin positive control. In agreement with these promising adhesion results, cell spreading reveals to be higher on PLCL fibers as opposed to the behavior observed on either on PLLA films, PLCL films, and PLLA fibers. However, all investigated samples allow the adhesion and the proliferation of the EC as compared to the Teflon surfaces

(negative control), which indicates a non-adherence and non-proliferation of the EC on the polymers surface for the first 4 days of culture.

3.7 HSVEC response to degradation products

Figure 8 shows cell toxicity outcomes after two and four days of cell spreading in the presence of degradation products for sample groups 9 to 14.

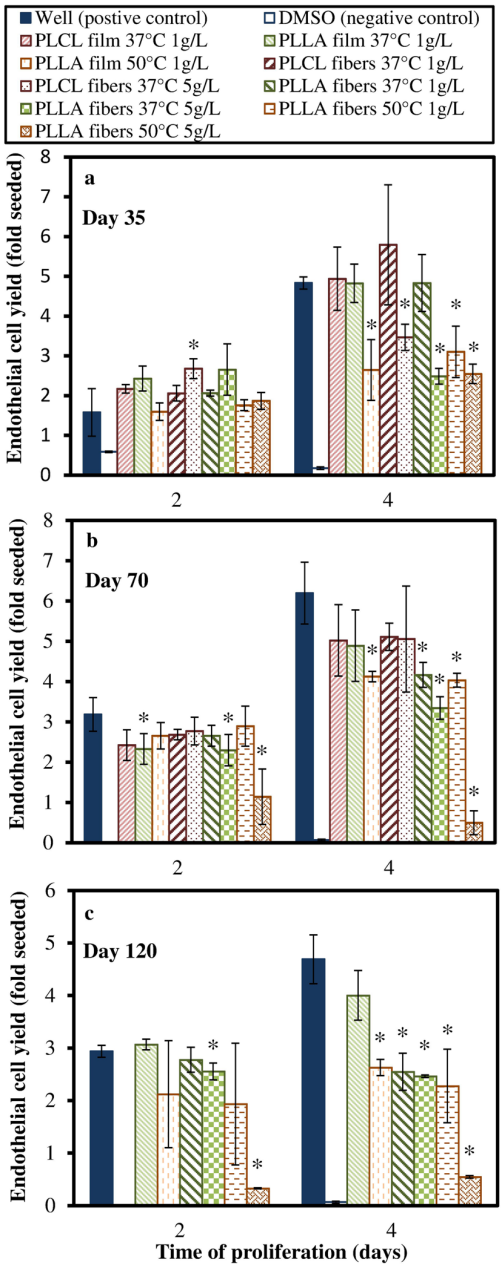

Figure 8. HSVEC response to sample degradation products after 35 days (a), 70 days (b) and 120 days (c) of degradation. The temperature and the mass to volume ratio correspond respectively to the degradation temperature and the fiber concentration in water during the degradation. * = significant difference ($p < 0.05$) as compared to the PP treated well according to Krurskal-Wallis ANOVA test.

After 35 days of degradation and 2 days of HSVEC proliferation (Figure 8a), HSVECs seems to proliferate well while in contact with every samples. Nonetheless, after 4 days of HSVEC proliferation, two distinct behaviors are observed with respect to the positive control. On one hand, PLCL film 37 °C 1 g/L, PLLA film 37 °C 1 g/L, PLCL fibers 37 °C 1 g/L and, PLLA fibers 37 °C 1 g/L lead to a HSVEC spreading similar to the PP well. On the other hand, PLLA film 50 °C 1 g/L, PLCL fibers 37 °C 5 g/L, PLLA fibers 37 °C 5 g/L, PLLA fibers 50 °C 1 g/L and, PLLA fibers 50 °C 5 g/L demonstrates an adverse and significant decrease in terms of HSVEC expansion. PLCL fibers 37°C 5 g/L shows a better HSVEC viability than PLLA fibers degraded either at 37 °C or 50 °C with a mass to volume ratio of 5 g/L.

After 70 days of degradation and 2 days of HSVEC proliferation (Figure 8b), no drastic difference in proliferation is observed between samples except for PLLA fibers 50 °C 5 g/L that show a lower EC yield which is, however, higher to the one observed in the DMSO solution. All samples exhibit EC proliferation lower than the positive control. After 4 days of spreading, PLCL film 37 °C 1 g/L, PLLA film 37 °C 1 g/L, PLCL fibers 37 °C 1 g/L, PLLA fibers 37 °C 1 g/L, PLLA film 50 °C 1 g/L, PLCL fibers 37 °C 5 g/L, PLLA fibers 37 °C 5 g/L and, PLLA fibers 50 °C 1 g/L exhibit similar EC proliferation yield than samples degraded for 35 days and PP treated well meaning that these samples show no adverse effect on HSVEC spreading. On the contrary, PLLA fibers 50 °C 5 g/L display behaviors that most resemble to those of the DMSO solution negative control, meaning that PLLA fibers degraded at 50 °C with a mass-to-volume ratio of 5 g/L are close to induce a cytotoxic response.

After 120 days of degradation and 2 and 4 days of proliferation (Figure 8c) in the presence of PLLA samples degradation products, HSVEC exhibit very similar behavior as 70 days of degradation.

Altogether, these results evidence that the PLLA degradation products, caused by the temperature-induced increase of PLLA degradation, have a negative impact on cell spreading. Nevertheless, none of these products demonstrate a cytotoxic behavior.

4 DISCUSSION

4.1 Design of PLLA and PLCL terpolymer air-spun nanofibers

PLLA is a widely acknowledged degradable polymer that is used in several biomedical applications [5]. However, it suffers from several drawbacks, which are related to its intrinsic molecular structure. PLLA is considered as a highly crystalline polymer, thus displaying a slow degradation and resorption rates. Additionally, it shows brittle behavior at body temperature, being clearly inappropriate for those applications requiring highly elastic properties. For these reasons, an amorphous PLCL was designed and compared with a PLLA polymer. In order to make the best possible comparison, both polymers were synthesized using conditions leading to similar molecular weights and distribution (table 2) and formed either as hot-pressed films with identical thickness or nanofiber scaffolds. PLLA reveals to be an excellent control material because it contains both amorphous and crystalline phases, therefore allowing evidencing the propensity of each of these phases to induce cell toxicity. In addition, its glass transition temperature is well above 37 °C, as opposed to that of PLCL, which permits to ascertain the importance of polymer chain mobility on its degradation. Finally, the degradation behavior of PLLA films is extremely well known and can be tailored [40] to match the PLCL degradation rate for a suitable comparison between the two materials.

Accordingly, accelerated degradation experiments were performed to understand the effect of the polymer macro and micro structures on hydrolytic degradation with a specific focus on the mechanisms of nanofibers degradation. In addition, adhesion and proliferation of HSVEC was assessed to evaluate the endothelial cell responses as a function of the same PLLA or PLCL level of degradation and to access which of these polymers would be the best candidate to be used as nanofiber scaffold for vascular biomaterials.

The new generation of PLCL terpolymer with distinctive features presented in this paper as basis material for air-spinning was also recently studied as film [31]. Copolymerization of L- or D-lactide with low glass transition temperature comonomers, such as ε-caprolactone, considerably improves elastic properties with respect to L- or D-lactide homopolymers. In addition, adding D-lactide units in L-lactide and ε-caprolactone based copolymers was shown to increase the amount of amorphous structure. Besides, modifying the monomer ratios allows fine-tuning of the polymer degradation rate from some days to some years. Lastly, controlling the length of L-lactide, D-lactide, and ε-caprolactone sequences during the polymerization process allows to prevent crystalline rearrangements at the beginning and during the hydrolysis reaction and, consequently, to a lower glass transition temperature [31]. Basically, BiSS catalyst was demonstrated to increase the randomness number and block crystalline phases formation as compared to more classical catalysts like stannous octoate [34].

Designing new prostheses for blood vessel replacement requires meeting specific criteria. Indeed, prostheses must be compliant, kink resistant and flexible [41]. These mechanical characteristics are all related to the elastic properties of the material used for fabricating prostheses. In addition, prostheses have to be biocompatible and easy to manufacture. First of all, the elastomeric films of the PLCL polymer developed in a previous study of our group [31] and recently patented [32] were shown to present better elastic properties than PLLA. Because these mechanical properties are generally improved after spinning and polymer scaffolds are aimed to temporarily replace the proteins of the extracellular matrix, it is worth comparing the mechanical properties of PLCL with common natural elastic proteins. For instance, the elastic modulus of PLCL is equal to 11 ± 1 MPa with an elongation at break of 300 % at 37 °C. By comparison, natural common elastic proteins have an elongation at break between 100 % and 200 %, while elastin of bovine ligament shows an elastic modulus of 11 MPa [42]. Concerning biocompatibility, polylactides and poly(ε-caprolactone) polymer films or nanofibers were extensively studied before degradation for decades [43,44] and used in biomedical applications, particularly in the vascular context. In addition, air-spun PLA nanofiber scaffold with a fiber diameter between 100 nm and 700 nm was proved to promote endothelial cell growth as monolayer [5], supplying a suitable structure to regenerate a functional endothelium. Figure 7 confirms these results by showing that the use of both PLCL and PLLA films and air-spun nanofiber scaffold are compatible with HSVEC adhesion and proliferation. Also, the air-spun PLCL nanofiber scaffold, presenting higher fiber diameters (Figure 6) but still in the sub-micrometer range, is evidenced to provide an appropriate scaffold surface for monolayer cell proliferation [45,46]. Finally, this work establishes the ease of adapting spinning parameters while changing polymer [20]. Meanwhile, the air-spinning process remains a useful, fast, cheap and safe route to produce non-woven nanofiber scaffold and, accordingly, could be easily scalable to industrial applications.

Working with degradable polymers for medical implant applications offers versatility in terms of temporary biological functionalities and drug delivery [47]. However, the non-cytotoxicity and biocompatibility of materials have to be investigated until completion of the degradation process. In this context, new specifications, related to the material degradation, have to be added to those initially required at the time of implantation [48]. For instance, crystallinity of PLA based polymers was questioned to play a role in acute foreign body reaction due to the accumulation of acidic by-products during the very long-term degradation of crystallites [49,50]. Furthermore, crystalline phases considerably delay the complete resorption of the device, which may reveal to be undesirable in the design of biomedical device requiring to be fully degraded in a specific period of time [51]. Because the crystalline phases of biodegradable PLA-based materials were somewhat adverse, the PLCL developed in the course of the present study is tailored to be amorphous throughout the degradation process, through appropriate control on the random distribution of the L-lactide, D-lactide, and ε-caprolactone along the polymer chain, with particular attention made on having short L-lactide sequences to avoid polymer crystallization during hydrolysis. Consequently, PLCL could be degraded faster, down to a molecular length of few monomers. At the end of the degradation,

polymeric short chains become soluble in biologic fluid and can then be easily metabolized by the body.

That said a unique polymer degradation rate may not be suited for all biomedical applications as it has to be tuned to take into account, of course, for the time required for cell proliferation, but also the strategy used for the device construction or the site of implantation. For example, strategies requiring in vitro cell seeding in scaffold-guided matrix need 2 weeks of static cell culture followed by 12 weeks in a bioreactor [3] for further in vivo neo-endothelialization for periods ranging between 2 and 24 weeks in rat, rabbit or dog models [52]. In vivo, polymer degradation could also be influenced by the mechanical conditions prevailing in the vasculature, such as the shear stress induced by the blood flow or the dilatation of the prosthesis [53]. This, in turn, is also likely to promote the delamination of the coating. Therefore, strategies for developing degradable scaffolds should take into account that degradation should occur after the proliferation of cells but before any delamination of the scaffold itself.

Considering aforementioned examples, PLCL constitutes an excellent candidate for vascular biomaterial applications because of its tunable degradation rate [31]. Indeed, PLCL films exhibits appropriate mechanical properties (Table 2) and remain amorphous from the beginning to the end of their degradation [33]. Finally, the use of appropriate synthesis conditions allows tuning the PLCL terpolymer degradation behavior. The PLCL presented in this study was designed to completely degrade after 12 weeks of in vitro hydrolysis degradation.

4.2 Degradation mechanisms

As expected, PLLA films degrade slower than their PLCL counterpart. Mechanism of film degradation is well described in the literature and attributed to bulk erosion [22,39,40]. First of all, water molecules diffuse inside the film, therefore leading to polymer chain scissions in the bulk material through hydrolysis. The hydrolysis of ester bonds leads, of course, to a polymer molecular weight decrease (Figure 1a) with, however, a constant overall weight of the polymer assembly (Figure 2a), therefore indicating the entrapment of acidic smaller polymer chains in the core of the material. This, in turn, auto-catalyzes the degradation process caused by a pH gradient decrease, which is proportional to the film thickness [54]. During random chain scission, shorter chains with higher mobility are produced and the entanglements between the polymer chains are reduced (leading to an increase in free volume). This increase in free volume facilitates water diffusion and that is the reason why water absorption increases together with the reduction of molecular weight. Finally, once the polymer chains reach a threshold value, they became soluble in aqueous medium with a concomitant decrease of the film weight.

Surprisingly, nanofiber scaffolds degrade slower than films at 37 °C as well as at 50 °C for both PLCL and PLLA polymers. This difference, evidenced by the half-life time required for ester bond hydrolysis reaction, is higher at 50 °C than at 37 °C for PLLA samples (Figure 1). These results support different mechanisms of degradation between films and fibers. Indeed, there is no reason to believe that bulk erosion could be more important in fibers than in films. However, the apparent higher porosity (Figures 5 and 6) of fibrous scaffold, and the higher specific surface area of nanofibers with respect to films, may be taken into account to lead to a decrease of degradation by-products entrapment, therefore facilitating their release in the media and consequently, reducing the auto-catalytic degradation rate.

The presence of a relaxation peak on DSC thermograms of PLLA nanofibers (Figures 3b and 3d) indicates a more organized and packed chain structure in the amorphous phase of the polymer, in agreement with a reduction in free volume over the degradation period [55]. The enthalpy associated to this relaxation peak was of 9.4 J/g for the PLLA fiber samples before degradation at 37°C, and readily stabilize to 15.4 J/g at day 14 up to the end of the investigated degradation period. This behavior signifies that the PLLA chains become more packed from the beginning of the degradation process (up to 14 days) and keep such a packing up to 70 days of degradation. Furthermore, the

gain in polymer chain mobility right after the T_g, combined to the presence of more ordered chain structures in the amorphous phase, favor the subsequent cold crystallization process that occurs just above the glass transition, as observed by an exothermic peak near 100°C. The packing of polymer chains in fibers therefore plays a role in their degradation mechanism by reducing diffusion of water in their core. Indeed, polymer chains within fibers are relatively oriented in the fiber axis forming an amorphous phase which is, however, capable to crystallize while heating. These typical phase has been previously described in the literature and was named interphase [56]. This organization induced by heating is not observed in the PLCL fiber thermograms because the synthesis conditions of PLCL lead to the absence of interaction between polymeric chains and hence, to the absence of organization (table 1). Despite a very low degradation rate, PLLA nanofibers undergo some changes like packing of polymer chains that can be visible and quantified by analyzing SEM images. For instance, fiber diameter distributions were evaluated and fitted with a log-normal curve, which allows determining the mode and the shape parameter of the distribution function. Regarding to PLLA nanofiber samples degraded at 37 °C, the mode of fiber diameter do not change significantly but the shape parameter decreased (result not shown), which is characteristic of a sharper distribution. Indeed, the population of larger fibers decreases and the number of fibers around the mode value increases, due to a packing of the polymer chains.

As previously mentioned, using nanofiber structure combined with their potential for biodegradation could be of interest for many biomedical applications. The fabrication of biodegradable polymer as nanofiber scaffold for these applications has been widely studied but, to our knowledge, the degradation behavior of PLA-based nanofiber scaffolds is poorly reported in the literature and rarely compared to standard sample like polymer films or pellets [57]. Because of a higher surface to volume ratio, nanofibers should intuitively degrade faster than films or macroscale polymeric device. However, the present study shows the opposite behavior. Indeed, bulk degradation mechanism of PLLA air-spun nanofibers, as compared with films, consists in the co-addition of two main effects that are porosity of scaffold leading to a decrease of the auto-catalysis process and the packing of polymer chains, which lead to a decrease of the water diffusion.

Because of the low degradation rate of polylactides, temperature-catalyzed degradation have been commonly used to shed more light on the degradation process of these polymers within reasonable delays [40,58,59]. In the present article, PLLA samples degradation has been accelerated by performing the experiments at 50 °C for 120 days to match the degradation rate of PLCL films at 37°C for 70 days (Figure 1) according to the model established by Weir et al [35]. This comparison between PLLA and PLCL films with the same degradation rate has been put forward to evaluate the influence of the crystalline phases and degradation products nature of PLCL and PLLA on the evolution of pH during the degradation process, as well as endothelial cell behavior. The relevance of this comparison is confirmed by the similar trends of PLLA films degraded at 50 °C and PLCL films degraded at 37 °C. DSC thermograms of PLLA films degraded at 50 °C (Figure 3c and 3e) highlight that the presence of shorter polymer chains with higher mobility may decrease the Tg below 50 °C, which, in turn, could lead to a drastic change in the degradation behavior. Indeed, a higher mobility of polymer chains occurred by overpassing T_g, leading to a greater penetration of water inside the film, which accelerates the degradation of amorphous phases and decrease the auto-catalytic effect due to a greater release of degradation products [60].

Regarding to the fiber samples degraded at 50 °C, the degradation rate is lower than that observed for films (Figure 1). In addition, the disappearance of the crystallization peak observed as a function of the degradation time (Figure 3d) confirms that the T_g of the polymer progressively decreased from a temperature higher than 50 °C to a temperature slightly below 50 °C over the investigated degradation period. Indeed, the mobility of chains, that is possible above T_g, and the presence of the previously mentioned interphases, induce the crystallization of PLLA fibers samples during the degradation. The degradation mechanism highlighted for PLLA nanofibers at 50 °C is also supported by the evolution of fiber morphology and the SEM image analysis (Figure 5). The increase of crystallinity index (figure 3e) due to the degradation of the amorphous phase is observed

as an important polymer morphology change from fibers to crumble-like samples. The mechanism described by Zong et al [61] for PLGA nanofiber degradation at 37 °C is fairly similar to the degradation of PLLA nanofibers at 50 °C. First of all, a degradation temperature above the T_g promotes the growth of crystalline phases. Then, water molecules penetrate in amorphous phases, degrades the nanofibers, and forms new smaller crystalline lamellae with higher hardness. Finally, nanofibers break down in smaller pieces. Our SEM analyses bring new information about this mechanism. As a matter of fact, the evolution of the fitted log-normal curve demonstrates that the mode and the shape parameter decrease. The slight increase of the shape parameter indicates a faster degradation of fibers with smaller diameters. Concomitantly, the decrease of the mode from 290 nm to 176 nm after day 70 may be related to the crystallization of bigger fibers, from a large amorphous domain to a smaller and more organized crystalline domain that reduce the free volume inside fibers. Finally, the stabilization of the mode value from day 70 to day 120 and the decrease of the degradation rate seem to arise from the shortening of nanofibers in the transverse direction. At this point, it is worth mentioning that nanofiber diameter distribution is often described as log-normal curve [62] but, to the best of our knowledge, the parameters that describe such a distribution, as the mode and shape parameter, was never used to quantify and understand the evolution of fiber morphology during degradation.

As opposed to PLLA degradation, PLCL nanofibers and PLCL films displays analogous degradation behaviors, as seen from Figures 1, 4 and previous article [33]. On one hand, these results can be explained because, as opposed to PLLA, no crystalline organization occurs in PLCL (Table 1). On the other hand, the evolution of PLCL nanofiber sample morphology upon degradation (Figure 6) shows that PLCL fibers merged in the early days of the degradation process with concomitant shrinking due to the presence of water. Indeed, water molecules easily penetrate inside the sample due to higher chain mobility, as evidenced by a T_g lower than 37 °C (Figure 4). This behavior is associated to the increase of fiber diameter (Figure 6g) and, consequently, a decrease of scaffold porosity [57]. Concomitantly, the shape parameter (Figure 6g) decreases as a function of degradation time, meaning that water diffuses easily in fibers leading to a larger diameter distribution. Fibers are then stuck between them, forming a continuous structure outside the sample after day 35, and leaving a porous structure inside the sample (Figure 6c and 6d). After day 70, samples become transparent (data not shown) and presents a morphology similar to a film (Figure 6e and 6f), with a degradation behavior characteristic of such sample morphology. In addition, Figure 3 confirms this statement by showing a slight increase of water absorption after 3 days of degradation that remains constant until 42 days of degradation. Moreover, after few days of degradation, the PLCL nanofiber samples behave like a film in terms of water absorption (Figure 2b), as opposed to PLLA nanofibers, which absorb a high amount of water because of the porosity of the scaffold. As a result, due to these early and non-reversible shrinkage and plasticizing effect of water, PLCL nanofibers samples and PLCL films display almost identical degradation behaviors.

The evolution of electrospun fiber morphology during their degradation was documented for PGA [63], semi-crystalline PLGA [61], amorphous PLGA [63], and semi-crystalline poly(L-lactide-co-ε-caprolactone) [63]. Altogether, these studies highlighted two types of evolution of nanofiber scaffold during the degradation. On one hand, nanofibers are semi-crystalline and break during the degradation or nanofiber material is totally amorphous and the scaffold shrinks during the degradation process above T_g. On the other hand, the percentage of shrinkage is directly related to the difference between T_g and the degradation temperature of the amorphous nanofibers. Results from Figures 5 and 6 are in agreement with these studies [57]. The degradation at 50 °C induces a crystallization of initially semi-crystalline PLLA nanofibers, leading to a contraction of amorphous phases, smaller fiber diameters, and early broken of fibers. On the contrary, PLCL nanofibers show an amorphous structure and the degradation at 37°C inducing a fast inflation of fibers without crystallization and, as a result, the porosity decreases, and the sample shrink. Finally, the degradation at 37 °C of semi-crystalline PLLA nanofibers allows evidencing another degradation mechanism. In this case, the degradation process at a temperature far below T_g is very slow due to

the packing of polymer chain. However, this packing increases during the degradation at 37 °C inducing a decrease of the number of the larger fibers.

By comparison with film or pellet degradation, studying degradable nanofiber brings additional information that allows understanding the evolution of fiber morphology features like porosity or diameter evolution during degradation.

4.3 Long-term cytotoxicity

Comparison of pH values (Table 3) between samples are in accordance with previously described degradation mechanisms. First, increase the degradation temperature from 37 °C to 50 °C lead to a decrease of pH values because of an increase of the degradation kinetics. Second, aqueous solutions containing PLCL sample degradation products are more acidic than those where PLLA is degraded at 37 °C because of the very low degradation rate of PLLA samples at this temperature. Nevertheless, the pH of the degradation medium over PLLA samples at 50 °C is lower than the one of PLCL samples at 37 °C, despite a similar degradation rate, meaning that degradation products made of lactic acid are more acidic than those arising from the degradation of caprolactone-based polymers. Third, PLLA fibers lead to more acidic degradation products than PLLA films at 37 °C since fiber degradation lead to fewer degradation by-product entrapments. On the contrary, the aqueous solution over PLLA fibers is less acidic than that over PLLA films at 50 °C due to the higher degradation rate of films as compared to fibers. Besides, aqueous media over PLCL fibers and films display almost identical pH values, in agreement with the fact that these samples degraded with a very similar kinetics and confirming the gradual conversion of fibers into films during the degradation process. Finally, degradation of fibers in a lower volume of water led to a lower pH value due to a higher concentration of degradation products. Finally, Table 2 shows that the buffer strength of M199 did not counterbalance the pH decrease induced by PLLA degradation at 50 °C, therefore indicating that the degradation of PLLA could lead to pH-induced cell toxicity.

Before degradation of samples, the level of HSVECs adhesion on PLCL and PLLA films and fibers is equivalent or even higher to that measured on the positive control (Figure 7a). Concerning proliferation results, every sample exhibits non-cytotoxic behavior (Figure 7b). HSVECs do not proliferate significantly on film after 4 days. However, nanofiber samples exhibit a more convenient environment for rapid HSVEC proliferation. These results also evidence that HSVEC spreading is clearly dependent on their adhesion rate on samples. Concerning PLA-based film samples, cells take more than 6 days to proliferate [64]. Besides, these results confirm, as widely acknowledged in the literature, that nanofiber scaffolds constitute more appropriate structures for cell spreading [6,9,52]. Finally, HSVEC adhesion on PLCL fibers is higher than that observed on either PLLA fibers, PP treated wells, and gelatinized wells, therefore highlighting the great potential of PLCL nanofiber scaffold for vascular tissue engineering and regenerative medicine applications.

The design and development of a biodegradable biomedical device require, evaluating its long term in vitro cytotoxicity. As demonstrated in this publication, polymeric device properties evolve all along the degradation. Indeed, the polymer molecular weight decreases with a concomitant modification of the polymer microstructure and scaffold morphology and by-product release, which lead to pH decrease of the cell culture media. This leads to a highly dynamic environment, where each of these evolving conditions may have a major influence on the cell fate.

The potential cytotoxicity and inappropriate tissue response of PLLA has been the subject of several in vitro studies as well as pre-clinical and clinical investigations [65]. Moreover, commercial or custom-made polylactide films possible toxicity was also evidenced in vitro with fibroblast cells [29,30]. All these studies concur to demonstrate that PLA films or pellets toxicity is due to an increase of crystallinity during its degradation, to the late degradation of crystalline phases, and to the inappropriate nature of degradation products leading to an important pH decrease. Indeed, PLA degradation behavior could lead to apoptosis, depending on cell tolerance to low pH [66]. Moreover, it is likely that the pH at which the cells are subjected is higher than the one that is experimentally

measurable since the local pH at the surface of implants is definitely higher than in the solution, therefore leading to more cell toxicity. In this context, PLCL seems to be a suitable alternative, which provides an appropriate HSVECs response to degradation products. The pH of the solutions over PLCL samples remains higher than over PLLA probably because PLCL remains amorphous throughout the degradation period. Finally, PLCL and its degradation products are demonstrated to have no effect on cell spreading. This polymer is therefore likely an excellent candidate for future tissue engineering applications in which tunable degradation rates are required.

5 CONCLUSION

This work investigates the possibility of using a PLCL terpolymer air-spun nanofiber scaffold for vascular tissue engineering and regenerative medicine applications. In addition to demonstrate appropriate elastomeric and structural properties, this novel PLCL terpolymer had a suitable degradation rate, which lead to its complete hydrolysis after 12 weeks without crystallization. A comparison between PLCL and PLLA nanofiber scaffolds and films upon degradation at 37°C allow getting a better understanding of the evolution of these polymer structural and dimensional features during the degradation. PLLA nanofibers exhibit a lower degradation rate than films because of the porosity inherent to the nanofibrous structure and the packing of polymer chains whereas PLCL films and nanofibers display very similar degradation rate and remain amorphous during all the degradation process. An accelerated degradation of PLLA nanofibers and films was performed at 50 °C to match the PLCL degradation rate. This enables to compare the impact of PLLA crystalline phase on the polymer degradation behavior with that of amorphous PLCL nanofibers. PLLA nanofibers degraded at 50 °C crystallize during the degradation process and present a brittle behavior while a rapid shrinkage is observed on PLCL nanofibers and, as a result, PLCL nanofibers readily behave as a film. In addition, the distributions of the nanofiber diameter evolution upon degradation were fitted with log-normal curves, which allow providing new insights of nanofiber degradation mechanisms. Finally, the increase of HSVEC adhesion on PLCL nanofibers, coupled with a non-cytotoxic effect of these polymer degradation products, indicates that PLCL is a suitable alternative to PLLA to produce nanofiber scaffold for vascular biomaterials.

ACKNOWLEDGEMENTS

The authors acknowledge Dr. Stephane Turgeon from CHU de Québec for his advices on statistical analyses and Arnaud De Coninck from ETE INRS of Quebec City for his SEM technical support. This work was co-supported by Region Alsace, the National Science and Engineering Research Council (NSERC) of Canada, and the Centre Québécois sur les Matériaux Fonctionnels (CQMF).

REFERENCES

1. A. S. Go *et al.*, *Circulation* **2013**, *127*, e6.
2. B. D. Ratner, S. J. Bryant, *Annu. Rev. Biomed. Eng.* **2004**, *6*, 41.
3. D. G. Seifu, A. Purnama, K. Mequanint, D. Mantovani, *Nat. Rev. Cardiol.* **2013**, *10*, 410.
4. S. François, N. Chakfé, B. Durand, G. Laroche, *Trends Biomater. Artif. Organs* **2008**, *2*, 93.
5. S. François, N. Chakfé, B. Durand, G. Laroche, *Acta Biomater.* **2009**, *5*, 2418.
6. S. Ramakrishna, K. Fujihara, W.-E. Teo, T.-C. Lim, Z. Ma, **2005**, *90*.
7. X. Zhang, M. R. Reagan, D. L. Kaplan, *Adv. Drug Deliv. Rev.* **2009**, *61*, 988.
8. S. Ramakrishna *et al.*, *J. Mater. Sci.* **2010**, *45*, 6283.
9. W. Liu, S. Thomopoulos, Y. Xia, *Adv. Healthc. Mater.* **2012**, *1*, 10.
10. S. Koombhongse, W. Liu, D. H. Reneker, *J. Polym. Sci. Part B Polym. Phys.* **2001**, *39*, 2598.
11. Z. Sun, E. Zussman, A. L. Yarin, J. H. Wendorff, A. Greiner, *Adv. Mater.* **2003**, *15*, 1929.

12. D. Li, Y. Xia, *Nano Lett.* **2004**, *4*, 933.
13. T. D. Brown, P. D. Dalton, D. W. Hutmacher, *Adv. Mater.* **2011**, *23*, 5651.
14. H. Yoshimoto, Y. M. Shin, H. Terai, J. P. Vacanti, *Biomaterials* **2003**, *24*, 2077.
15. S. G. Kumbar, S. P. Nukavarapu, R. James, L. S. Nair, C. T. Laurencin, *Biomaterials* **2008**, *29*, 4100.
16. X. Zong *et al.*, *Biomaterials* **2005**, *26*, 5330.
17. C. Li, C. Vepari, H.-J. Jin, H. J. Kim, D. L. Kaplan, *Biomaterials* **2006**, *27*, 3115.
18. M. Shin, H. Yoshimoto, J. P. Vacanti, *Tissue Eng.* **2004**, *10*, 33.
19. J. Xie *et al.*, *Biomaterials* **2009**, *30*, 354.
20. G. Sabbatier, P. Abadie, F. Dieval, B. Durand, G. Laroche, *Mater. Sci. Eng. C* **2014**, *35*, 347.
21. S. François *et al.*, *J. Biomed. Mater. Res. Part B Appl. Biomater.* **2010**, *93*, 531.
22. M. Treiser, S. Abramson, R. Langer, J. Kohn, *Biomater. Sci. (Third Ed. An Introd. to Mater. Med.* **2013**, 179, doi:http://dx.doi.org/10.1016/B978-0-08-087780-8.00021-8.
23. E. J. Frazza, E. E. Schmitt, *J. Biomed. Mater. Res.* **1971**, *5*, 43.
24. N. R. Ko, G. Sabbatier, A. Cunningham, G. Laroche, J. K. Oh, *Macromol. Rapid Commun.* **2014**, *35*, 447.
25. J. Iqbal, J. Gunn, P. W. Serruys, *Br. Med. Bull.* **2013**, *106* , 193.
26. G. Sabbatier *et al.*, *Polym. Degrad. Stab.* **2012**, *97*, 1520.
27. J. Fernández, A. Larrañaga, A. Etxeberría, J. R. Sarasua, *Polym. Degrad. Stab.* **2013**, *98*, 481.
28. C. A. P. Joziasse *et al.*, *Colloid Polym. Sci.* **1998**, *276*, 968.
29. F. W. Cordewener *et al.*, *Biomaterials* **2000**, *21*, 2433.
30. J. R. Sarasua *et al.*, *J. Mater. Sci. Mater. Med.* **2011**, *22*, 2513.
31. J. Fernández, A. Larrañaga, A. Etxeberria, W. Wang, J. R. Sarasua, *J. Biomed. Mater. Res. Part A* **2013**, *102*, 1.
32. J. Fernández, A. Larrañaga, J.-R. Sarasua, **2014**, at <http://www.google.com/patents/WO2014135727A1?cl=en>.
33. A. Larrañaga *et al.*, *Biomatter* **2014**, *4*, e27979.
34. J. Fernández *et al.*, *Polymer (Guildf).* **2013**, *54*, 2621.
35. N. Weir, F. J. Buchanan, J. F. Orr, D. F. Farrar, G. R. Dickson, *Proc. Inst. Mech. Eng. Part H J. Eng. Med.* **2004**, *218*, 321.
36. J. Fernández, A. Etxeberria, J.-R. Sarasua, *J. Mech. Behav. Biomed. Mater.* **2012**, *9*, 100.
37. J.-R. Sarasua, R. E. Prud'homme, M. Wisniewski, A. Le Borgne, N. Spassky, *Macromolecules* **1998**, *31*, 3895.
38. M.-C. Boivin *et al.*, *J. Biomed. Mater. Res. A* **2013**, *101*, 694.
39. C.-C. Lin, K. S. Anseth, *Biomater. Sci. (Third Ed. An Introd. to Mater. Med.* **2013**, 716, doi:http://dx.doi.org/10.1016/B978-0-08-087780-8.00061-9.
40. H. Tsuji, *Poly (lactic acid) Synth. Struct. Prop. Process. Appl.* **2011**, *10*.
41. O. E. Teebken, A. Haverich, *Eur. J. Vasc. Endovasc. Surg.* **2002**, *23*, 475.
42. J. Gosline *et al.*, *Philos. Trans. R. Soc. Lond. B. Biol. Sci.* **2002**, *357*, 121.
43. K. A. Athanasiou, G. G. Niederauer, C. M. Agrawal, *Biomaterials* **1996**, *17*, 93.
44. M. C. Serrano *et al.*, *Biomaterials* **2004**, *25*, 5603.
45. A. S. Badami, M. R. Kreke, M. S. Thompson, J. S. Riffle, A. S. Goldstein, *Biomaterials* **2006**, *27*, 596.
46. M. Chen, P. K. Patra, S. B. Warner, S. Bhowmick, *Tissue Eng.* **2007**, *13*, 579.
47. H. Tian, Z. Tang, X. Zhuang, X. Chen, X. Jing, *Prog. Polym. Sci.* **2012**, *37*, 237.
48. J. C. Middleton, a J. Tipton, *Biomaterials* **2000**, *21*, 2335.
49. M. S. Taylor, A. U. Daniels, K. P. Andriano, J. Heller, *J. Appl. Biomater.* **1994**, *5*, 151.
50. S. J. Yoon *et al.*, *Tissue Eng. Part A* **2008**, *14*, 539.
51. J. M. Anderson, M. S. Shive, *Adv. Drug Deliv. Rev.* **2012**, *64*, 72.
52. K. A. Rocco, M. W. Maxfield, C. Best, E. W. Dean, C. K. Breuer, *Tissue Eng.* **2014**, *20*, 628.

53. J. Choi *et al.*, *Langmuir* **2011**, *27*, 14232.
54. K. Fu, D. W. Pack, a M. Klibanov, R. Langer, *Pharm. Res.* **2000**, *17*, 100.
55. S. Petisco, A. Larrañaga, C. Gracia, J. Sarasua, *Eurotech* **2013**, 488.
56. R. Picciochi, Y. Wang, N. Alves, J. Mano, *Colloid Polym. Sci.* **2007**, *285*, 575.
57. Y. Dong, S. Liao, M. Ngiam, C. K. Chan, S. Ramakrishna, *Tissue Eng. Part B. Rev.* **2009**, *15*, 333.
58. S. R. Andersson, M. Hakkarainen, S. Inkinen, A. Södergård, A.-C. Albertsson, *Biomacromolecules* **2010**, *11*, 1067.
59. H. Tsuji, T. Tsuruno, *Polym. Degrad. Stab.* **2010**, *95*, 477.
60. A. Gleadall, J. Pan, M.-A. Kruft, M. Kellomäki, *Acta Biomater.* **2014**, *10*, 2223.
61. X. Zong *et al.*, *Biomacromolecules* **2003**, *4*, 416.
62. J. S. Varabhas, G. G. Chase, D. H. Reneker, *Polymer (Guildf).* **2008**, *49*, 4226.
63. Y. Dong *et al.*, *Tissue Eng. Part A* **2009**, *16*, 283.
64. A. van Sliedregt, A. M. Radder, K. de Groot, C. A. van Blitterswijk, *J. Mater. Sci. Mater. Med.* **1992**, *3*, 365.
65. O. Böstman, H. Pihlajamäki, *Biomaterials* **2000**, *21*, 2615.
66. D. Sgouras, R. Duncan, *J. Mater. Sci. Mater. Med.* **1990**, *1*, 61.